Pseudogap and electron localization in the 4*d* shell of NbO_2 bulk crystal

L. Craco[1,2] and M. S. Laad[3]
[1]*Institute of Physics, Federal University of Mato Grosso, 78060-900 Cuiabá, MT, Brazil*
[2]*Leibniz Institute for Solid State and Materials Research Dresden, D-01069 Dresden, Germany*
[3]*Institute of Mathematical Sciences, Chennai 600113, India*

(Received 1 June 2023; revised 27 September 2023; accepted 2 November 2023; published 17 November 2023)

We present a detailed study of correlation-induced electronic reconstruction in NbO_2 bulk crystal. Using density functional plus dynamical mean-field theory (DFT+DMFT), we show the importance of multiorbital Coulomb interactions in concert with first-principles band structure calculations for a consistent understanding of emergent pseudogap and incipient Mott localization in NbO_2. We explain the pseudogapped incoherent metal to a Mott-localization-like transition seen in experiment. We trace its origin to changes in orbital polarization, itself renormalized from its DFT value by sizable multiorbital electron correlations. Our results should be of interest for future studies on electronic switching in Mott memristors for neuromorphic computing devices.

DOI: 10.1103/PhysRevB.108.205137

I. INTRODUCTION

Understanding the subtleties of correlation-induced Mott metal-insulator transition [1] remains a problem of enduring interest in condensed matter and material physics [2,3]. One of the most prominent examples within the transition-metal dioxide family are the vanadium oxides, in particular VO_2, which undergoes a first-order metal-insulator transition around room temperature [4]. The high-T metallic phase has tetragonal rutile-type structure, which is reduced to monoclinic at the first-order transition occurring around 340 K [2]. Mott-Hubbard (dynamical correlations) [1] and Peierls (structural distortion) [5] mechanisms are understood to play essential roles, and possibly to work in concert in this transition since the lattice distortion appears to be assisted [6–8] by the presence of strongly correlated electronic states in close proximity to Mottness [9–11]. In this work we show that a dynamically reconstructed many-particle electronic state induced by multiorbital (MO) electron-electron interactions [12,13] plays a central role in determining the orbital-selective nature of rutile NbO_2. This system may be close to an insulating state due to reduced screening [9] and enhanced orbital polarization [14,15] effects caused by changes in crystal-field splitting [16], especially under perturbations such as strain. Motivated thereby, based on density functional plus dynamical mean-field-theory (DFT+DMFT) calculations [17], we show how the electronic structure of rutile NbO_2 [14,15] is reshaped due to sizable electron-electron interactions in the real crystal structure. In light of earlier studies [12,18–21], we revisit the issue of how the electronic structure of rutile NbO_2 [14,15] is reconstructed by MO dynamic correlations, showing an emergent pseudogap regime as the precursor of a Mott localized state in distorted rutile [body centered tetragonal (bct)] NbO_2 as a result of enhanced electron correlation and orbital polarization effects. [22]

Similar to VO_2, under ambient pressure conditions NbO_2 undergoes a metal-insulator transition at temperatures between 810 and 1081 K [3,20,23], which comes along with a structural transition from the low-temperature, semiconducting distorted rutile ($I4_1/a$) structure to a metallic regular rutile ($P4_2/mnm$) structure [24]. The niobium atoms are formally in the Nb^{4+} oxidation state with a valence configuration of $4d^1$ [13,25], being therefore an isovalent with $3d$ VO_2. While the precise mechanism of the structural transition [19] and the nature of the metal-insulator transition in NbO_2 and analogs [3] is debated, dimerization of the Nb ions along the c direction in distorted rutile may naturally lead to a band gap in the low-T electronic structure [14,15,20,26] in the framework of a bonding-antibonding splitting within DFT [5]. However, on very general grounds, one expects MO correlation effects to control electronic structure evolution, an aspect completely missed in DFT studies.

NbO_2 is presently regarded as a promising material for applications in memory devices [27] and neural-inspired computing [28–30]. The neuromorphic computing framework was motivated by the discovery of a Mott-based memristor that replicates the voltage-triggered switching behavior observed in biological ion channels enabling a physical neuristor circuit to be built [31]. NbO_2 memristors are known to successfully replicate the rectification observed in voltage-gated biological ion channels [32] and the hysteresis necessary for operation of the proposed neuristor circuit [31]. Interestingly, metal-insulator-metal devices based on niobium oxides have shown to exhibit the rectification and hysteresis necessary for high-density neuristor circuitry without the need to electroform a conducting filament [30,33]. Moreover, nanoscale devices with the annealed NbO_2 films show bulk crystallization and uniform resistivity with large threshold voltages [34], supporting the view that NbO_2 is a promising candidate for future memristive devices for neuromorphic computing [29].

The evolution of electronic spectra and band gap formation across the metal-insulator transition in NbO_2 has been experimentally explored in recent years [20,21,25,35,36]. Reference [20] shows a metallic state with pseudogaplike features at low energies evolving into a localized state at lower temperature (T). In the insulator, the $4d$ valence band is narrowed

and shifted downward by approximately 0.4 eV across the structural phase transition, which, according to Ref. [20], is second-order Peierls-driven metal-insulator transition. This result is, however, in contrast with nonthermal, photoinduced metallic state reported in Ref. [25], where photodoping of holes in the valence band causes an instantaneous collapse of the band gap without structural modification of the metastable metallic phase. This later study together with ultrafast photoemission measurements on VO_2 [37], constitute evidence for the dominantly electronic character of the metal-insulator transition [21] in NbO_2 and transition-metal dioxide analogs.

Theoretically, the influence of dynamical electron correlations on the electronic properties of both rutile and bct phase of NbO_2 were addressed in Ref. [12]. According to this density functional theory plus cluster-dynamical mean-field theory (DFT+cDMFT) study, electronic correlations lead to strong renormalization of the t_{2g} bands and the emergence of incoherent Hubbard bands. Moreover, consistent with prior theoretical DFT work [19], this DFT+cDMFT study suggests that structural distortions are not solely responsible for the gap opening of the bct phase, ruling out a purely Peierls-type nature for the insulating phase. The role played by MO electronic correlations within the rutile phase of normal and strained NbO_2 were also studied using DFT implemented with the slave spin method (DFT+SS) [21]. Thereby, the band structure is modified by the elongation of the c axis by driving more electrons in the $d_{x^2\text{-}y^2}$ orbital due to interband and interorbital hybridization. Since extant DFT studies neglect the dynamical nature of the interplay between local Hubbard interactions and the band kinetic energy, the role played by MO electron-electron interactions in the electronic structure reconstruction and gap formation due to changes in screening [9,38] along with orbital polarization [11,22] and orbital splitting [39] in NbO_2 remains to be clarified. Here, we shed light onto this issue, showing that like VO_2, NbO_2 may be an ideal material to study the mechanisms of metal-insulator transition triggered by orbital-selective Mottness in concert with dimerization, itself favored on structural grounds.

II. RESULTS AND DISCUSSION

As in VO_2 [9], we here argue that the pseudogap observed in rutile NbO_2 [20] is intrinsic and signals its proximity to Mottness. To explore this, we use orbital-resolved DFT results for the metallic structure computed in Ref. [14] using the scalar-relativistic augmented spherical wave (ASW) method [40] with lattice constants and atomic positions obtained for rutile-type structure [24], as input to DFT+DMFT [17]. The projected density of states (DOS) of Fig. 1 shows that the active electronic states in this $4d^1$ rutile compound are the Nb-t_{2g} carriers [14,15], where all $4d - t_{2g}$ bands have appreciable spectral weight near the Fermi energy, $E_F = \omega = 0$. As displayed in Fig. 1 and similar to Ref. [15], the t_{2g} (xz, yz, x^2-y^2) orbitals show metallic behavior with finite DOS near E_F in contrast to the higher-energy e_g orbitals [15], which are semiconducting due to large bonding-antibonding splitting in the conduction band states above E_F [15]. An interesting aspect in the bare DFT DOS is the nearly one-dimensional-like dispersion of the x^2-y^2 orbital parallel to the rutile c axis [14]. Moreover, while the xz DOS shows a single broad structure,

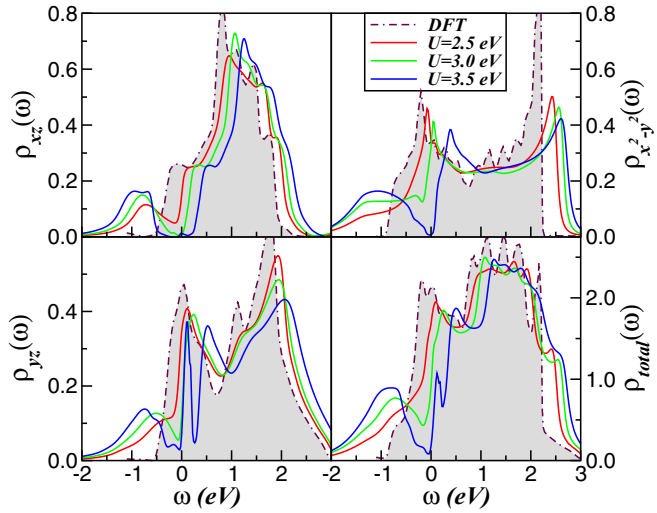

FIG. 1. Comparison between DFT [14] and DFT+DMFT orbital resolved and total density of states (DOS) for the t_{2g} orbitals of rutile NbO_2. While all t_{2g} bands span across the Fermi level, an important feature to be seen is the pseudogap [20] behavior at E_F and the emergence of lower Hubbard bands with increasing the on-site Coulomb interaction U. While the metal-insulator transition in NbO_2 is found at temperatures between 810 and 1081 K [3,20,23], here all DFT+DMFT (MO-IPT) spectral functions are computed at zero temperature to avoid thermal broadening effects.

the yz DOS displays a two maxima structure, although less pronounced as compared to that for the x^2-y^2 orbital. The restructuring of the t_{2g} orbitals with nearly one- (x^2-y^2, yz) and two-dimensional-like (xz) spectral functions by local dynamical correlations in concert with changes in orbital polarization (note that these two effects self-consistently reinforce each other) due to orbital splitting effects in the rutilelike structure must hold the key to understanding the metal-insulator transition, and this is our focus below.

The one-electron Hamiltonian part of rutile NbO_2 is $H_0 = \sum_{\mathbf{k},a,\sigma} \epsilon_a(\mathbf{k}) c^\dagger_{\mathbf{k},a,\sigma} c_{\mathbf{k},a,\sigma} + \sum_{i,a,\sigma} (\epsilon^{(0)}_{a,\sigma} - \mu) n_{i,a,\sigma} + \Delta \sum_{i,\sigma} (n_{i,xz,\sigma} - n_{i,x^2\text{-}y^2,\sigma})$, where $a = (x^2\text{-}y^2, yz, xz)$ denote the diagonalized t_{2g} orbitals of rutile NbO_2 [14]. In the usual notation, $c^\dagger_{\mathbf{k},a,\sigma}$ ($c_{\mathbf{k},a,\sigma}$) are the creation (annihilation) operators for electrons in orbital a and momentum $\mathbf{k}$, with spin $\sigma(=\uparrow,\downarrow)$ and $n_{i,a,\sigma} = c^\dagger_{i,a,\sigma} c_{a,i,\sigma}$ is the occupation number operator of an a-orbital state with spin σ at site i. $\epsilon_a(\mathbf{k})$ is the DFT band dispersion, which encodes details of the bare-t_{2g} band structure and $\epsilon^{(0)}_{a,\sigma} \equiv \epsilon_a - U(n_{a,\bar{\sigma}} - \frac{1}{2}) + \frac{J_H}{2}(n_{a,\sigma} - 1)$. ϵ_a is the on-site energy of a given $3d$ orbital and the other terms are subtracted therefrom to avoid double counting of interactions already treated on average by DFT [41], and μ is the chemical potential of the system. Within our MO scheme, the orbital field Δ [42] (sometimes also referred to as crystal-field splitting parameter) [43] simulates the changes in the t_{2g} orbital occupancies across the structural phase transition of NbO_2 [14,15], and $n_{i,xz,\sigma} = n_{i,yz,\sigma}$. These are relevant inputs for MO DFT+DMFT, which generically reconstructs the t_{2g} bands across the metal-insulator transition. Local MO interactions in NbO_2 are contained in $H_{\rm int} = U \sum_{i,a} n_{i,a,\uparrow} n_{i,a,\downarrow} + U' \sum_{i,a\neq b} n_{i,a} n_{i,b} - J_H \sum_{i,a\neq b} \mathbf{S}_{i,a} \cdot \mathbf{S}_{i,b}$,

where U is the on-site Coulomb interaction, $U' = U - 2J_H$ is the interorbital Coulomb interaction term, and J_H is the Hund's coupling. We evaluate the one-particle Green's functions of the MO Hamiltonian $H = H_0 + H_{\rm int}$ within DFT+DMFT [17], using MO iterated perturbation theory (MO-IPT) as impurity solver [44]. The DMFT solution involves replacing the lattice model by a self-consistently embedded MO-Anderson impurity model, and the self-consistency condition requiring the local impurity Green's function to be equal to the local Green's function for the lattice. The full set of equations for the MO case can be found in Ref. [44], so we do not repeat the equations here.

Let us now discuss our DFT+DMFT results for NbO_2. In Fig. 1 we display the effect of electron-electron interactions on the active x^2-y^2, xz, yz orbitals and the total spectral function $[\rho_{\rm total}(\omega) = \sum_{a,\sigma} \rho_{a,\sigma}(\omega)]$ of rutile $(\Delta = 0.0)$ NbO_2. For $U = 2.5$ eV (and $J_H = 1.0$ eV) [45], rutile NbO_2 is on the metallic side of the correlated phase diagram [2]. Upon increasing the on-site U from 2.5 to 3.0 eV, we uncover an orbital-selective electronic state with coexisting pseudogapped (incoherent metallic) (yz, x^2-y^2) and Mott localized (xz) electrons. (For the sake of clarity, we point out that pseudogap in DMFT refers to a loss of coherent low-energy electronlike quasiparticles due to a correlation-induced depression of electronic states near E_F [46].) Moreover, at $U =$ 3.5 eV the Mott gap of the xz orbital increases in size and also emerges in the x^2-y^2 channel. In this particular correlated electron regime, the yz states remain pseudogaplike at low energies. In this parameter range, lower (LHB) and upper (UHB) Hubbard bands are visible in all-t_{2g} orbital-resolved spectral functions. As seen, while the x^2-y^2 orbital shows more pronounced LHB at $U = 3.5$ eV reflecting a ground-state character with large orbital occupancy, the more metallic yz states are less prone to local moment formation (LHB). These changes must also be reflected in the total spectral function.

In order to shine light onto the effect of MO electron-electron interactions in rutile NbO_2, we show in Fig. 2 the frequency dependence of the orbital-resolved self-energies imaginary (main panels) and real (insets) parts for the U values considered in Fig. 1. At $U = 2.5$ eV $\mathrm{Im}\Sigma_a(\omega)$ shows ω^2 dependence characteristic of good Fermi-liquid metals. However, as shown in Fig. 1, this canonical correlated electronic state evolves into an orbital-selective electronic state at $U = 3.0$ eV with coexisting insulating (xz) and metallic (yz, x^2-y^2) channels. Due to orbital-selective Mottness, at $U =$ 3.0 eV the xz orbital now acts as a localized moment to the yz, x^2-y^2 channels responsible for the incoherent metallicity via U', J_H-induced interorbital proximity effect. This in turn indicates the presence of strong MO correlations within the orbital-selective metallic phase of rutile NbO_2. Also, remarkable in Fig. 2 is the ω dependence of $\mathrm{Re}\Sigma_a(\omega)$, which depends strongly on frequency at low energies as reported for VO_2 [10].

To analyze dynamical MO correlation effects in rutile NbO_2, we display the changes in the orbital-resolved spectral functions induced by increasing U from 3.5 to 4.5 eV in Fig. 3. The latter is consistent with the effective strength parameter $U_{\rm eff} \equiv U - J = 5.0$ eV reported in Ref. [47]. As seen in Fig. 3, MO electronic correlations lead to large modifications in spectra. At $U = 4.5$ eV and $\Delta = 0.0$ eV

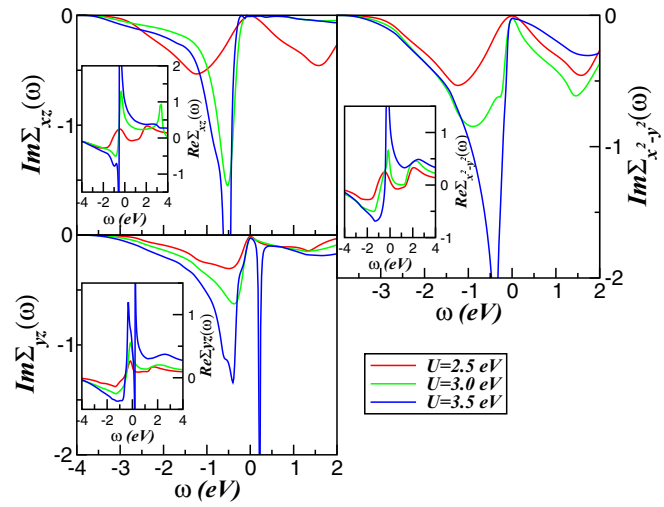

FIG. 2. Orbital-resolved self-energies imaginary (main panels) and real (insets) parts of NbO_2 bulk crystal, showing their evolution with increasing the on-site Coulomb interaction U. Particular features to be seen are the Fermi-liquid-like behavior for $U = 2.5$ eV and its suppression with increasing U. Also interesting is the particle-hole asymmetry [13] and the presence of poles in the self-energy imaginary parts [12].

the many-body spectra describe an orbital-selective metal with orbital-dependent Mott localized and narrow low-energy one-particle features in the xz, yz, and x^2-y^2 orbital states. Noteworthy is the suppression of the one-electron itinerance at low energies and the emergence of a well-defined LHB at energies close to -0.78 eV for the yz band, and clear reconstruction of the shoulder feature above E_F for the xz band, both as consequences of sizable dynamic spectral weight transfer upon increasing U.

In Fig. 3, we also display the changes in the DFT+DMFT spectra upon consideration of sizable orbital field effects: these originate from the distortions in the rutile phase of NbO_2, [42] and could be engineered experimentally by controlled strain tuning [21]. Within our MO DFT+DMFT scheme, consideration of the orbital field Δ in the one-electron Hamiltonian H_0 is motivated by extant *ab initio* DFT studies [14,15], showing the emergence of a strongly orbital polarized electronic state across the metal-insulator transition in NbO_2. While in the rutile phase the t_{2g} orbitals are all partially filled, within the distorted rutile phase the x^2-y^2 orbital is pushed down in energy and becomes nearly half-filled while the xz, yz orbitals are nearly empty. Thus, within our theoretical framework the effect of the structural distortion was deduced based on DFT results by changing the difference in the centers of gravity of the different t_{2g} bands upon consideration of the orbital field Δ. With these caveats and similar to earlier work [9,48], we use the following strategy to study the electronic phase transition in NbO_2. Since we do not expect much correspondence between changes in the bare DFT quantities with those affected in nontrivial ways by dynamical electronic correlations, we choose the bare DFT DOS for the metallic solution. We do not change this DOS to study the electronic transition at low temperatures in our calculation [14,15], but vary the t_{2g} orbital occupancies (themselves dictated in reality

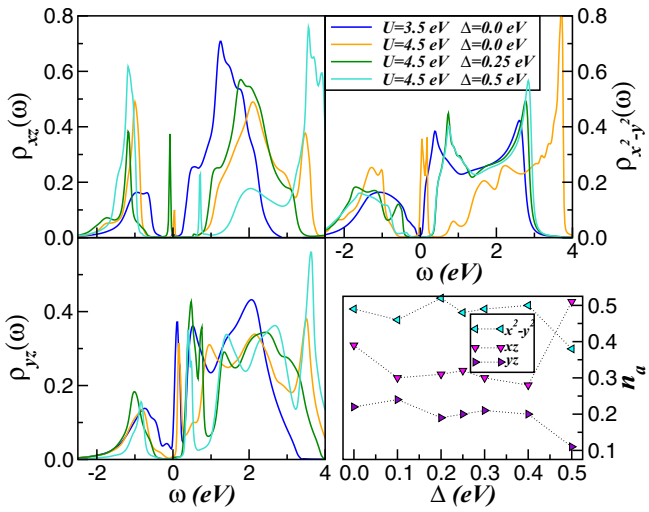

FIG. 3. Orbital-resolved DFT+DMFT DOS of NbO_2, showing their evolution with increasing U. Apart from orbital-selective Mott localization at $U = 3.5$ eV in the regular rutile phase ($\Delta = 0.0$ eV), a particular interesting feature to be seen is the large spectral weight transfer for $U = 4.5$ eV and $\Delta = 0.0$ eV within the xz and x^2-y^2 orbitals. Also noteworthy is the evolution of the orbital-resolved DOS of distorted rutile NbO_2 with increasing the orbital field Δ for fixed $U = 4.5$ eV. Apart from Mott localization, a relevant feature to be seen is the spectral weight transfer among different orbitals with increasing Δ. Right-lower panel displays the Δ dependence of the Nb-t_{2g} orbital occupations n_a. Notice the orbital switching, inducing enhanced charge carrier concentration in the xz channel above $\Delta_c = 0.42$ eV.

by the correlation-enhanced crystal-field splittings) to monitor the fully renormalized spectral functions along with their renormalized occupations within DFT+DMFT. Nontrivial changes induced by MO correlations have two important effects: given a trial value of Δ, static effects (Hartree) of U, U', J_H generically renormalize the bare value of the effective orbital field acting on the t_{2g} sector via MO Hartree shifts, inducing changes in the orbital occupations, and more importantly, to large changes in spectral weight transfer driven by the dynamical nature of strong local correlations upon changes in Δ, leading to stabilization of the second [9] DFT+DMFT solution, as shown below. In other words, this large spectral weight transfer drives an orbital switching around a critical value of $\Delta_c = 0.42$ eV (see bottom-right panel of Fig. 3), similar to that reported for VO_2 [22]. Also interesting in Fig. 3 is the electronic reconstruction of the x^2-y^2 orbital obtained for $U = 4.5$ eV and $\Delta = 0.0$ eV. As a result of our self-consistent MO DFT+DMFT calculation a well-separated single band with clear van Hove singularities at the edges emerges around E_F at $U = 4.5$ eV and $\Delta = 0.0$ eV. Interestingly, although not a completely isolated narrow band as we have derived for $U = 4.5$ eV and $\Delta = 0.0$ eV, a quasi-one-dimensional-like feature near E_E is also seen in Ref. [12] for the $e_g(2)$ orbital of rutile NbO_2, suggesting similar MO reconstruction for the strongly correlated electronic state of NbO_2 bulk crystal. Our result in Fig. 3 for $U = 4.5$ eV and $\Delta = 0.0$ eV can thus be taken as a many-particle platform for realizing nearly flat-band quantum phenomena and possibly correlated topological states [49] in NbO_2 and analogs.

As shown in Fig. 3, at $U = 4.5$ eV and finite Δ we find a Mott insulator. This occurs concurrently with an abrupt orbital rearrangement for Δ between 0.4 and 0.5 eV, accompanied by a switch in the orbital occupations [48,50] of the x^2-y^2 and xz orbitals, and is a direct consequence of the intricate interplay between correlation and structural aspects in MO systems. As seen in the bottom-right panel of Fig. 3, while the yz orbital loses it spectral weight the second DFT+DMFT solution obtained at $\Delta = 0.5$ eV is characterized by a reversal of orbital polarization between the x^2-y^2 and the xz orbital. The latter shows enhanced spectral weight below E_F, as visible in top-left panel of Fig. 3. These large spectral weight transfers allow an understanding of the unconventional electronic structure reconstruction in NbO_2. Manifestations thereof in soft x-ray absorption spectroscopy [22] and K-edge x-ray magnetic circular dichroism [51] studies across the metal-insulator transition in NbO_2 would also be of interest.

Interestingly, our results in Fig. 3 seems to suggest a link between orbital and the electronic switching across the metal-insulator transition, which might introduce a history-dependent resistance needed for neuromorphic computing devices [29]. Experimentally, NbO_2-based Mott memristors each less than 100 nanometres exhibit both a nonlinear transport-driven current-controlled negative differential resistance and a Mott-transition-driven temperature-controlled negative differential resistance [29]. We recall that in their experimental setup [29], Kumar *et al.* incorporate the NbO_2 memristors into a relaxation oscillator, showing that the nonlinear current transport coupled with thermal fluctuations at the nanoscale generates chaotic oscillations. Thus, due to the nanometer scale size of the NbO_2 Mott memristors the metal-insulator transition that acts as an electronic switch, which in turn introduces a history-dependent resistance into the device, might have a different origin as compared to the Mott-assisted Peierls transition of bulk NbO_2 [12]. Our results in Fig. 3 suggest a link between the presence of hidden orbital polarized ground states and the electronic switching behavior needed for neuromorphic computing. Within this context, we mention here that the current-voltage profiles based on NbO_2 memristor devices, the current suddenly increases when the voltage reached the threshold voltage [52], suggesting that the switching mechanism of NbO_2 needed for future neuromorphic computing is not a high-T-driven insulator-metal transition but by the changes of orbital polarized ground states in the electrically induced insulator-metal transition [53]. We plan to explore the interplay between low-T orbital fluctuations and electric field effects in future Mott memristors studies.

Next, in Fig. 4, we show the U and Δ dependence of the self-energy imaginary (main panels) and real (insets) parts associated with the active 4d orbitals of NbO_2. Comparing our results to that reported for the bct phase of NbO_2 [12], we notice similar particle-hole asymmetry in $\Sigma_a(\omega)$. This particle-hole asymmetry is manifested by the appearance of peaks below E_F in $\mathrm{Im}\Sigma_a(\omega)$, which are strongly enhanced going over to pole structures with increasing U. Also interesting is the emergence of poles in $\mathrm{Im}\Sigma_a(\omega)$ at and above E_F similar to those obtained using cellular cluster DMFT (c-DMFT)

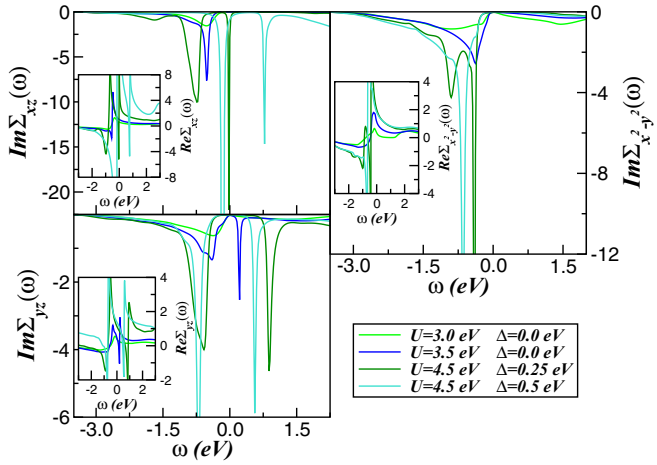

FIG. 4. Orbital-resolved self-energies imaginary (main panels) and real (insets) parts of NbO_2, showing their evolution with increasing the on-site Coulomb interaction U and the orbital field Δ. Particular features to be seen are the clearly visible particle-hole asymmetry and the presence of poles associated with Mott localization in the self-energy imaginary parts [12].

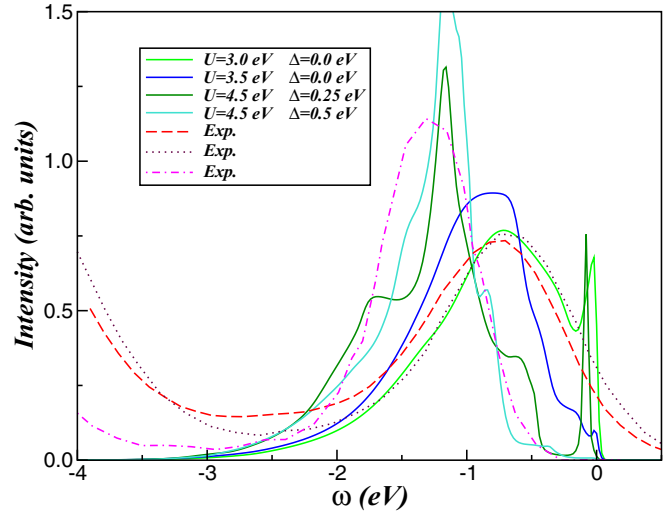

FIG. 5. Theory-experiment comparison between the DFT+DMFT results and hard x-ray photoelectron spectroscopy (HAXPES) measurements taken from Refs. [21] (dashed curve) and [20] (dot and dot-dashed curves). The dashed and doted curves correspond to the regular rutile phase. Notice the good qualitative theory-experiment agreement between 0.2 and 2.5 eV binding energy, particularly the peak position of the lower Hubbard band for the rutile and bct phases.

calculations for VO_2 [7], a clear signature of a similar Mott instability in both systems. The observation of these sharp poles close to E_F, together with $\mathrm{Im}\Sigma_a(\omega = E_F) = 0$ supports the view that the Mott instability of NbO_2 is prevented once the dimerization occurs [12]: For the sake of clarity we notice here that Mott localization is usually associated with the presence of poles in the self-energy imaginary part at or near the Fermi energy, as pointed out in Refs. [12,54] among other studies. Thus, since in our results for $U = 4.5$ eV we do observe poles in the self-energy imaginary parts, the insulating state at finite Δ shown in Fig. 3 can be characterized as a Mott-assisted insulating state, consistent with the DFT+cDMFT results of Ref. [12]. Moreover, as in VO_2 structural effects that tend to reduce the Nb-Nb distance would be expected to be better screened in the incoherent metal than in the Mott insulator (where they are essentially unscreened). This should directly enhance the crystal-field splitting, favoring the tendency to dimerization as a direct consequence. Once dimerization occurs, one may expect the insulator to be adiabatically continuable to a renormalized (Kondo) band Peierls insulator. Our finding of $\mathrm{Im}\Sigma_a(\omega = E_F) = 0$ is in full qualitative accord with this reasoning. However, as can be seen in the insets of Fig. 4, the real part of self-energies also have a pronounced frequency dependence near E_F: This implies strong renormalization of DFT bandwidths, in accord with Ref. [12]. These findings constitute clear evidence for the important role of the interplay between electronic correlations and structural distortions in driving the electronic structure reconstruction of NbO_2.

Finally, to rationalize the overall correlated electronic behavior of NbO_2, in Fig. 5 we compare our DFT+DMFT results with extant hard x-ray photoelectron spectroscopy (HAXPES) spectra for the rutile [20,21] and the bct [20] structural phases of NbO_2. As seen, good qualitative agreement between theory and experiment is found over the entire range of $-2.5 \leqslant \omega \leqslant -0.2$ eV. In particular, the energy position of the LHBs for the rutile and bct phases as well as the narrow line shape and enhanced intensity of the bct spectra as compared to the rutile one are all in good qualitative agreement with experiment in spite of different crystal structures and model parameters values. Thus, our theory-experiment comparison represents a qualitatively accurate representation of the valence one-electron spectral function of NbO_2.

While our DFT+DMFT results provide good qualitative description of the metallic and insulating phases, they give only a limited description of the c-axis dimerized insulating state. This shortcoming has to do with the intrinsic inability of single-site DMFT itself to treat dynamical correlations associated with the quasi-one-dimensional Peierls transition seen in the distorted rutile phase of NbO_2 and analogs. This needs an extension to a two-site cluster-DMFT calculation, and we have not done it here. Our description is nonetheless expected to provide new insights to photoinduced [25] metal-insulator transition, which, we propose, is driven by large spectral weight transfer from low to high energy accompanying increase in crystal-field splitting.

III. CONCLUSION

In summary, we have employed density functional theory combined with dynamical mean-field theory (DFT+DMFT) to analyze the electronic structures of rutile and distorted rutile phase of NbO_2. We have shown that sizable electron-electron correlation and orbital polarization (structural effects) drives orbital-selective modifications of the quasiparticle spectra, generating emergence of incoherent electronic spectra in the single-particle spectral functions. The interplay between these two distinct effects pushes distorted NbO_2 towards a switching of the orbital occupation: this could be the precursor for

the Mott-assisted Peierls instability [6–8]. Our work should be of interest in studies of the voltage [55] or electronic [29] switching mechanisms relevant to future scalable neuristors built with Mott memristors [31] incorporating early transition-metal dioxides.

ACKNOWLEDGMENT

Acknowledgment (L.C.) is made to CAPES and CNPq as well as to S. S. Carara for helpful comments and P. Z. de Arruda for useful discussions.

[1] N. F. Mott, Rev. Mod. Phys. **40**, 677 (1968).
[2] M. Imada, A. Fujimori, and Y. Tokura, Rev. Mod. Phys. **70**, 1039 (1998); See also, B. H. Brandow, Adv. Phys. **26**, 651 (1977).
[3] D. Adler, Rev. Mod. Phys. **40**, 714 (1968).
[4] Z. Shao, X. Cao, H. Luo, and P. Jin, NPG Asia Mater. **10**, 581 (2018).
[5] J. B. Goodenough, J. Solid State Chem. **3**, 490 (1971).
[6] S. Biermann, A. Poteryaev, A. I. Lichtenstein, and A. Georges, Phys. Rev. Lett. **94**, 026404 (2005).
[7] C. Weber, D. D. O'Regan, N. D. M. Hine, M. C. Payne, G. Kotliar, and P. B. Littlewood, Phys. Rev. Lett. **108**, 256402 (2012).
[8] F. Grandi, A. Amaricci, and M. Fabrizio, Phys. Rev. Res. **2**, 013298 (2020) and references therein.
[9] M. S. Laad, L. Craco, and E. Müller-Hartmann, Phys. Rev. B **73**, 195120 (2006).
[10] W. H. Brito, M. G. O. Aguiar, K. Haule, and G. Kotliar, Phys. Rev. Lett. **117**, 056402 (2016).
[11] S. Kim, S. Backes, H. Yoon, W. Kim, C. Sohn, J. Son, S. Biermann, T. W. Noh, and S. Y. Park, npj Quantum Mater. **7**, 95 (2022).
[12] W. H. Brito, M. G. O. Aguiar, K. Haule, and G. Kotliar, Phys. Rev. B **96**, 195102 (2017).
[13] L. Craco and S. Leoni, Phys. Rev. B **102**, 045142 (2020).
[14] V. Eyert, Europhys. Lett. **58**, 851 (2002).
[15] K. Kulmus, S. Gemming, M. Schreiber, D. Pashov, and S. Acharya, Phys. Rev. B **104**, 035128 (2021).
[16] T. Mizokawa, New J. Phys. **6**, 169 (2004); See also, S. Leoni, A. N. Yaresko, N. Perkins, H. Rosner, and L. Craco, Phys. Rev. B **78**, 125105 (2008).
[17] G. Kotliar, S. Y. Savrasov, K. Haule, V. S. Oudovenko, O. Parcollet, and C. A. Marianetti, Rev. Mod. Phys. **78**, 865 (2006).
[18] A. O'Hara, T. N. Nunley, A. B. Posadas, S. Zollner, and A. A. Demkov, J. Appl. Phys. **116**, 213705 (2014).
[19] A. O'Hara and A. A. Demkov, Phys. Rev. B **91**, 094305 (2015).
[20] M. J. Wahila, G. Paez, C. N. Singh, A. Regoutz, S. Sallis, M. J. Zuba, J. Rana, M. B. Tellekamp, J. E. Boschker, T. Markurt, J. E. N. Swallow, L. A. H. Jones, T. D. Veal, W. Yang, T.-L. Lee, F. Rodolakis, J. T. Sadowski, D. Prendergast, W.-C. Lee, W. A. Doolittle *et al.*, Phys. Rev. Mater. **3**, 074602 (2019).
[21] W.-C. Lee, M. J. Wahila, S. Mukherjee, C. N. Singh, T. Eustance, A. Regoutz, H. Paik, J. E. Boschker, F. Rodolakis, T.-L. Lee, D. G. Schlom, and L. F. J. Piper, J. Appl. Phys. **125**, 082539 (2019).
[22] M. W. Haverkort, Z. Hu, A. Tanaka, W. Reichelt, S. V. Streltsov, M. A. Korotin, V. I. Anisimov, H. H. Hsieh, H.-J. Lin, C. T. Chen, D. I. Khomskii, and L. H. Tjeng, Phys. Rev. Lett. **95**, 196404 (2005).
[23] R. F. Janninck and D. H. Whitmore, J. Phys. Chem. Solids **27**, 1183 (1966); R. Pynn and J. D. Axe, J. Phys. C: Solid State Phys. **9**, L199 (1976); K. Seta and K. Naito, J. Chem. Thermodyn. **14**, 921 (1982); see also, J. Stoever, J. E. Boschker, S. B. Anooz, M. Schmidbauer, P. Petrik, J. Schwarzkopf, M. Albrecht, and K. Irmscher, Appl. Phys. Lett. **116**, 182103 (2020).
[24] A. A. Bolzan, C. Fong, B. J. Kennedy, and C. J. Howard, J. Solid State Chem. **113**, 9 (1994); K. Momma and F. Izumi, J. Appl. Cryst. **44**, 1272 (2011).
[25] R. Rana, J. M. Klopf, J. Grenzer, H. Schneider, M. Helm, and A. Pashkin, Phys. Rev. B **99**, 041102(R) (2019).
[26] G. J. P. Fajardo, S. A. Howard, E. Evlyukhin, M. J. Wahila, W. R. Mondal, M. Zuba, J. E. Boschker, H. Paik, D. G. Schlom, J. T. Sadowski, S. A. Tenney, B. Reinhart, W.-C. Lee, and L. F. J. Piper, Chem. Mater. **33**, 1416 (2021).
[27] S. Kim, J. Park, J. Woo, C. Cho, W. Lee, J. Shin, G. Choi, S. Park, D. Lee, B. H. Lee, and H. Hwang, Microelectron. Eng. **107**, 33 (2013); E. Cha, J. Park, J. Woo, D. Lee, A. Prakash, and H. Hwang, Appl. Phys. Lett. **108**, 153502 (2016).
[28] Y. Ran, Y. Pei, Z. Zhou, H. Wang, Y. Sun, Z. Wang, M. Hao, J. Zhao, J. Chen, and X. Yan, Nano Res. **16**, 1165 (2023).
[29] S. Kumar, J. P. Strachan, and R. S. Williams, Nature (London) **548**, 318 (2017).
[30] J. C. Shank, M. B. Tellekamp, M. J. Wahila, S. Howard, A. S. Weidenbach, B. Zivasatienraj, L. F. J. Piper, and W. A. Doolittle, Sci. Rep. **8**, 12935 (2018).
[31] M. D. Pickett, G. Medeiros-Ribeiro, and R. S. Williams, Nat. Mater. **12**, 114 (2013).
[32] B. Connors, M. Gutnick, and D. Prince, J. Neurophysiol. **48**, 1302 (1982).
[33] The NbO_2 memristors are manufactured by electroforming an insulating layer of Nb_2O_5 into the semiconductor NbO_2.
[34] M. C. Sullivan, Z. R. Robinson, K. Beckmann, A. Powell, T. Mburu, K. Pittman, and N. Cady, J. Vac. Sci. Technol. B **40**, 063202 (2022); See also, P. Chen, X. Zhang, Q. Liu, and M. Liu, Appl. Phys. A **128**, 1113 (2022).
[35] A. B. Posadas, A. O'Hara, S. Rangan, R. A. Bartynski, and A. A. Demkov, Appl. Phys. Lett. **104**, 092901 (2014).
[36] J. K. Clark, Y.-L. Ho, H. Matsui, H. Tabata, and J.-J. Delaunay, Phys. Rev. Res. **1**, 033168 (2019).
[37] D. Wegkamp, M. Herzog, L. Xian, M. Gatti, P. Cudazzo, C. L. McGahan, R. E. Marvel, R. F. Haglund, Jr., A. Rubio, M. Wolf, and J. Stähler, Phys. Rev. Lett. **113**, 216401 (2014).
[38] D. Wegkamp and J. Stähler, Prog. Surf. Sci. **90**, 464 (2015).
[39] F. J. Wong, N. Hong, and S. Ramanathan, Phys. Rev. B **90**, 115135 (2014).
[40] A. R Williams, J. Kübler, and C. D. Gelatt, Jr., Phys. Rev. B **19**, 6094 (1979).
[41] V. I. Anisimov, A. I. Poteryaev, M. A. Korotin, A. O. Anokhin, and G. Kotliar, J. Phys.: Condens. Matter **9**, 7359 (1997).

[42] Δ is the energy difference between the one-electron energy levels between the x^2-y^2 and xz, yz orbitals relevant to determine the electronic reconstruction across the rutile to distorted rutile structural phase transition in NbO_2.

[43] L. Craco, M. S. Laad, and E. Müller-Hartmann, Phys. Rev. B **74**, 064425 (2006) and reference therein; See also, L.-F. Lin, Y. Zhang, G. Alvarez, M. A. McGuire, A. F. May, A. Moreo, and E. Dagotto, Commun. Phys. **6**, 199 (2023).

[44] L. Craco, Phys. Rev. B **77**, 125122 (2008).

[45] We use the same J_H value as in Refs. [12,13,21].

[46] M. R. Norman, D. Pines, and C. Kallin, Adv. Phys. **54**, 715 (2005); G. Sordi, P. Sémon, K. Haule, and A.-M. S. Tremblay, Phys. Rev. Lett. **108**, 216401 (2012).

[47] Y. Liu, H. Zhang, and X. Cheng, Comput. Mater. Sci. **173**, 109434 (2020).

[48] L. Craco, M. S. Laad, S. Leoni, and H. Rosner, Phys. Rev. B **77**, 075108 (2008).

[49] L. Chen, F. Xie, S. Sur, H. Hu, S. Paschen, J. Cano, and Q. Si, arXiv:2212.08017.

[50] M. S. Laad, L. Craco, and E. Müller-Hartmann, Phys. Rev. Lett. **91**, 156402 (2003).

[51] E. Goering, A. Bayer, S. Gold, G. Schütz, M. Rabe, U. Rüdiger, and G. Güntherodt, Europhys. Lett. **58**, 906 (2002).

[52] See, for example, A. Chen, Y. Fu, G. Ma, G. Yang, N. Liu, X. Zhao, Z. Zhang, L. Tao, H. Wan, Y. Rao, J. Duan, L. Shen, J. Zhang, P. Sun, D. Yang, T.-C. Chang, and H. Wang, IEEE Electron Dev. Lett. **43**, 870 (2022).

[53] J. del Valle, R. Rocco, C. Domínguez, J. Fowlie, S. Gariglio, M. J. Rozenberg, and J.-M. Triscone, Phys. Rev. B **104**, 165141 (2021).

[54] P. Yue and P. Werner, arXiv:2303.16888.

[55] M. D. Goldflam, M. K. Liu, B. C. Chapler, H. T. Stinson, A. J. Sternbach, A. S. McLeod, J. D. Zhang, K. Geng, M. Royal, B.-J. Kim, R. D. Averitt, N. M. Jokerst, D. R. Smith, H.-T. Kim, and D. N. Basov, App. Phys. Lett. **105**, 041117 (2014).